Timelike virtual compton scattering from electron-positron radiative annihilation

Andrei Afanasev,[1] Stanley J. Brodsky,[2] Carl E. Carlson,[3] and Asmita Mukherjee[4]
[1]*Department of Physics, Hampton University, Hampton, Virginia 23668, USA,*
and Theory Center, Thomas Jefferson National Accelerator Facility, 12000 Jefferson Avenue, Newport News, Virginia 23606, USA
[2]*SLAC National Accelerator Laboratory, Stanford University, Stanford, California 94309, USA*
[3]*Department of Physics, College of William and Mary, Williamsburg, Virginia 23187, USA*
[4]*Department of Physics, Indian Institute of Technology, Powai, Mumbai 400076, India*
(Received 29 July 2009; published 10 February 2010)

We propose measurements of the deeply virtual Compton amplitude (DVCS) $\gamma^* \to h\bar{h}\gamma$ in the timelike $t = (p_h + p_{\bar{h}})^2 > 0$ kinematic domain which is accessible at electron-positron colliders via the radiative annihilation process $e^+e^- \to h\bar{h}\gamma$. These processes allow the measurement of timelike deeply virtual Compton scattering for a variety of $h\bar{h}$ hadron pairs such as $\pi^+\pi^-$, K^+K^-, and $D\bar{D}$ as well as $p\bar{p}$. As in the conventional spacelike DVCS, there are interfering coherent amplitudes contributing to the timelike processes involving $C = -$ form factors. The interference between the amplitudes measures the phase of the $C = +$ timelike DVCS amplitude relative to the phase of the timelike form factors and can be isolated by considering the forward-backward $e^+ \leftrightarrow e^-$ asymmetry. The $J = 0$ fixed pole contribution which arises from the local coupling of the two photons to the quark current plays a special role. As an example we present a simple model.

DOI: 10.1103/PhysRevD.81.034014 PACS numbers: 13.66.Bc, 13.40.Gp, 13.60.Fz

I. INTRODUCTION

Deeply virtual Compton scattering (DCVS) $\gamma^*(q) + p(p) \to \gamma(k) + p(p')$, where the virtuality of the initial photon $-q^2$ is large, measures hadronic matrix elements of the current commutator $\langle p'|[J^\mu(x), J^\nu(0)]|p\rangle$ and has become a key focus in QCD, because of its direct sensitivity to fundamental hadron structure. Assuming the handbag approximation [1], interactions between the virtual and real photons can be ignored, so that at large spacelike q^2 one measures matrix elements of elementary quark commutators $\sum e_q^2\langle p'|j_q^\mu(x), j_q^\nu(0)]|p\rangle$ and each DVCS helicity amplitude factorizes as a convolution in x of the hard $\gamma^* q \to \gamma q$ Compton amplitude with a hadronic subamplitude constructed from the generalized parton distributions (GPDs) $H(x, \xi, t)$, $E(x, \xi, t)$, $\tilde{H}(x, \xi, t)$, and $\tilde{E}(x, \xi, t)$. Here x is the light cone momentum fraction of the struck quark, and the skewness $2\xi = Q^2/(2P \cdot q)$ measures the longitudinal momentum transfer in the DVCS process.

The DVCS helicity amplitudes can be constructed in the light-front formalism from the overlap of the target hadron's light-front wave functions [2,3]. Since the DVCS process involves off-forward hadronic matrix elements of light-front bilocal currents, the overlaps are in general nondiagonal in particle number, unlike ordinary parton distributions. Thus in the case of GPDs, one requires not only the diagonal parton number conserving $n \to n$ overlap of the initial and final light-front wave functions, but also an off-diagonal $n + 1 \to n - 1$ overlap, where the parton number is decreased by two. Thus the GPDs measure hadron structure at the amplitude level in contrast to the probabilistic properties of parton distribution functions. In the forward limit of zero momentum transfer, the GPDs reduce to ordinary parton distributions; on the other hand, the integration of GPDs over x at fixed skewness $2\xi = Q^2/2P \cdot q$ reduces them to electromagnetic and gravitational form factors. One also obtains information on the orbital angular momentum carried by quarks.

The Fourier transform of the deeply virtual Compton scattering amplitude with respect to the skewness parameter $2\xi = Q^2/2P \cdot q$ can be used to provide an image of the target hadron in the boost-invariant variable σ, the coordinate conjugate to light-front time $\tau = t + z/c$ [4,5]. The Fourier Transform of the GPDs with respect to the transverse momentum transfer $\Delta_\perp$ in the idealized limit $\xi = 0$ measures the impact parameter dependent parton distributions $q(x, b_\perp)$ defined from the absolute squares of the hadron's light-front wave functions in x and impact space [6–10].

Virtual Compton scattering is normally measured in radiative electron-proton scattering $ep \to e'\gamma p'$, where the photon virtuality $q^2 = (p'_e - p_e)^2 < 0$ and the momentum transfer to the target proton $t = (p' - p)^2 < 0$ are spacelike. The real part of the DVCS amplitude can be measured by using the interference with the coherent Bethe-Heitler bremsstrahlung contribution where the real photon is emitted from the lepton in $ep \to e'\gamma p'$. The interference of the DVCS amplitude and the coherent Bethe-Heitler amplitude leads to an $e^\pm$ asymmetry which is related to the real part of the DVCS amplitude [11]. The imaginary part can also be accessed through various spin asymmetries [12]. In the deep inelastic inclusive case, the electron-positron beam asymmetry gives a three-current correlator which is sensitive to the cube of the quark charges [13].

In this paper we will discuss possible measurements of the DVCS amplitude in the timelike or $t > 0$ kinematic

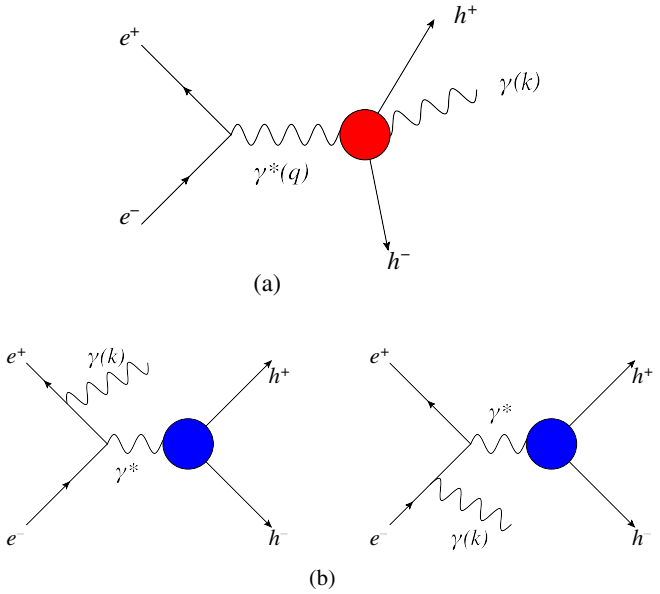

FIG. 1 (color online). Processes contributing to $e^+e^- \to h^+h^-\gamma$: (a) the generic timelike DVCS process and (b) Bethe-Heitler processes.

domain, where $t = W^2 = (p_h + p_{\bar{h}})^2$ is the mass of the produced hadron pair. The process we consider is the radiative annihilation process $e^+e^- \to h\bar{h}\gamma$ [14], which is accessible at electron-positron colliders and measures the timelike DVCS amplitude $\mathcal{M}(\gamma^*(q) \to \gamma h\bar{h})$ illustrated in Fig. 1(a). We focus on $p\bar{p}$ hadronic pairs, but many of the considerations apply for a variety of $h\bar{h}$ hadron pairs including $\pi^+\pi^-$, K^+K^-, and $D\bar{D}$. The hadronic matrix element is C even since two photons attach to it. The same final state can also come from Bethe-Heitler processes, Fig. 1(b), where the hadronic part of the matrix element is C odd.

One can apply charge conjugation the electron and positron in the initial state, thus relating two kinematic situations where the momentum and spin of the electron and positron are interchanged. The amplitudes change sign or not depending on the photon attachment to the initial electron line. The asymmetry obtained by interchanging the electron and positron is sensitive to the interference term between the C-even and C-odd amplitudes as

$$A = \frac{\sigma - \sigma(e^+ \leftrightarrow e^-)}{\sigma + \sigma(e^+ \leftrightarrow e^-)} = \frac{2\,\mathrm{Re}(\mathcal{M}^\dagger(C=+) \times \mathcal{M}(C=-))}{|\mathcal{M}(C=+)|^2 + |\mathcal{M}(C=-)|^2}, \quad (1)$$

which is sensitive to the relative phase of the C-even DVCS amplitude and the timelike form factors.

The cross sections and amplitudes above are for fixed final state momenta with the electrons interchanged. In the center-of-mass (CM) frame, the result of electron-positron exchange can also be obtained (at least in the unpolarized case) by a 180° rotation about a suitable axis. Hence one can obtain the same asymmetry A from fixed electron and positron momenta and rotating all the final state momenta.

The QED equivalents of these amplitudes, where hadrons are replaced by muons, usefully show that the magnitude of the $e^+ \leftrightarrow e^-$ asymmetry can be quite large.

Regarding related processes, another timelike DVCS process [15] can also be accessed using electron-positron colliders. This is doubly virtual DVCS, where one uses $e^+e^- \to e^+e^-h\bar{h}$ to measure the amplitude $\mathcal{M}(\gamma^*(q)\gamma^*(q') \to h\bar{h})$ with one or both initial photons

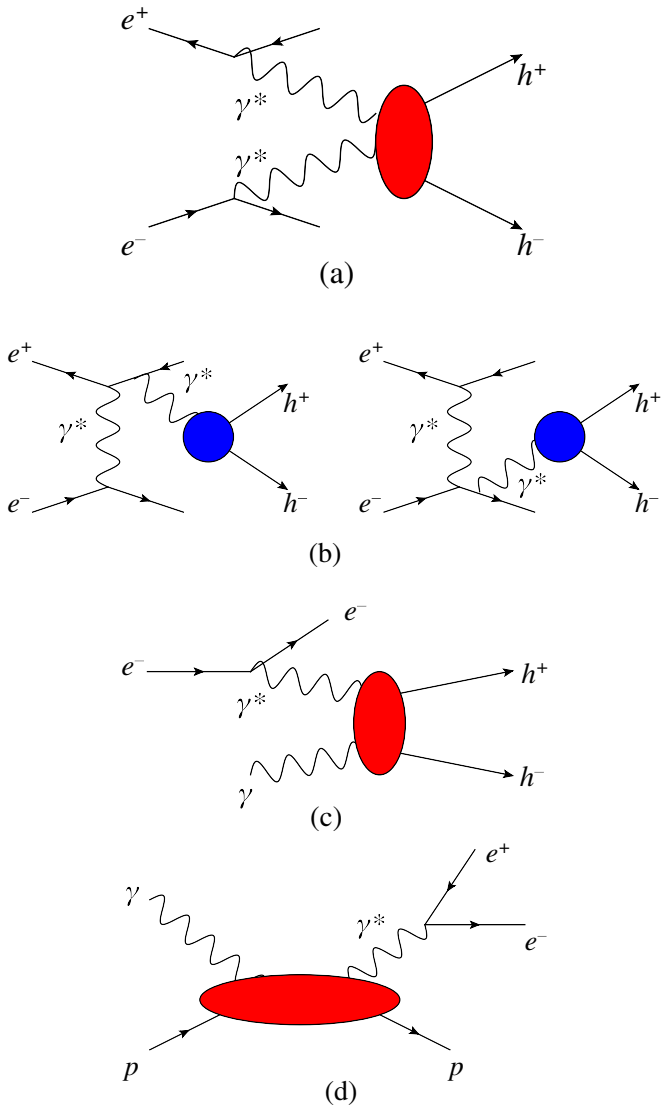

FIG. 2 (color online). Other processes of interest: (a) doubly virtual timelike DVCS; (b) Bethe-Heitler processes interfering with doubly virtual timelike DVCS; (c) production of hadron pairs with one spacelike virtual photon and one real photon; and (d) a process with a timelike photon, but with spacelike momentum transfer to the hadron, which here is already present in the initial state.

highly spacelike, as illustrated in Fig. 2(a). This process also has interfering Bethe-Heitler companion processes leading to the same final state, Fig. 2(b). We defer further consideration of the doubly virtual process to a future discussion.

Another related process is shown in Fig. 2(c). It is the production of hadron pairs from photon pairs where one photon is virtual, but in contrast to our process is spacelike rather than timelike, and the other photon is real, but again in contrast to our process is incoming rather than outgoing. This process is studied in Ref. [16] for outgoing pions. These authors give the amplitude in terms of a two-hadron matrix element that they call the ''generalized distribution amplitude,'' which we might prefer to call a timelike generalized parton distribution, and whose analog we discuss in Sec. II C.

The description ''timelike Compton scattering'' has also been applied to the process $\gamma p \to e^+ e^- p$ [17], Fig. 2(d), which is timelike in the sense that the outgoing photon is timelike. However, this process still has spacelike momentum transfer to the nucleon, and so measures nucleon information complementary to what we are targeting here. Also, having a preexisting nucleon allows modeling based on known parton distribution functions, a type of modeling which is not possible here.

Returning to the topic of this paper, we present a model calculation of the asymmetry for kinematic conditions of existing electron-positron colliders. Relevant kinematics is chosen for tau-charm factories, $s = 14\ \mathrm{GeV}^2$ (BEPCII) and B-factories, $s = 112\ \mathrm{GeV}^2$ (*BABAR* at PEPII and Belle at KEKB) [18]. The increased luminosity of the electron-positron colliders, such as the projected SuperB facility [19], will facilitate studies of the exclusive reactions at high transferred momenta, an example of which is considered in our paper. We note that the use of a radiative return method (see Ref. [20] and references therein) would allow studies of the reaction of interest in a broad range of Mandelstam s.

Measurements of the radiative annihilation process can provide valuable new information on the analytic continuation of the DVCS amplitude. A feature expected for photon-hadron amplitudes is a $J = 0$ fixed pole, which would be an amplitude that is constant in energy (and real in the spacelike case) though not constant in momentum transfer. The fixed pole has no analog in purely hadronic reactions [21–24]. It occurs because the hadron has pointlike constituents and it comes from a configuration where both photons attach locally to the same quark propagator.

(This term is the seagull interaction in the case of charged scalar quarks. The same local two-photon interaction also emerges for spin-1/2 from the usual handbag Feynman diagram for Compton scattering. The numerator of the quark propagator $\gamma \cdot k_F + m$ appearing between the two photons in the handbag contributions to the Compton amplitude contains a specific term $\gamma^+ \delta k^-/2$ which cancels the $k_F^2 - m^2$ Feynman denominator, leaving a local term inversely proportional to k^+. This can also be identified with the instantaneous fermion exchange contribution in the light-front Hamiltonian formulation of QCD [25]. Thus in the spin-1/2 case, the two-photon interaction is local in impact space and light-front time $\tau = x^+ = x^0 + x^3$, but it is nonlocal in the light-front coordinate $\sigma = x^- = x^0 - x^3$.)

In the case of ordinary spacelike DVCS this local contribution is universal, giving the same contribution for real or virtual Compton scattering for any photon virtuality and skewness at fixed momentum transfer squared t. The t dependence of this $J = 0$ fixed Regge pole is given by a yet unmeasured even charge-conjugation form factor of the target nucleon. In the spacelike region, this gives an amplitude which behaves as $s^0 F^+(t)$ for $s \gg -t$ corresponding to a local scalar probe. One can analytically continue the $J = 0$ amplitude to a local form independent of photon virtuality at fixed t. It is characterized by a complex timelike form factor $F^+(t = W^2 > 0)$ dominated by scalar meson resonances.

We obtain a simple hadronic estimate by modeling the C-even $p\bar{p}$ timelike hadronic DVCS amplitude after an analysis of how it can be written in terms of several Lorentz structures multiplied by $C = +$form factors. One of these is $R_V(\xi, W^2)$ and all of these can be related to the timelike generalized parton distributions, or generalized distribution amplitudes [15,16]. We will keep only the R_V term, which has the appearance of the QED amplitude multiplied by $R_V(\xi, W^2)$, and we will model this form factor in a simplified way where it depends only on $W^2 = t = (q - q')^2$ and is independent of s, or the overall q^2. One can say that this model simulates the C-even Compton amplitude as a $J = 0$ fixed pole amplitude with Regge behavior s^0 at fixed t.

Of relevance here is an experimental result for the spacelike $C = +$form factor $R_V(t)$ from real wide-angle Compton scattering. It is defined as the ratio of the measured real Compton amplitude $M(\gamma p \to \gamma' p')$ divided by the pointlike Klein-Nishina formula. $R_V(t)$ is measured to fall off as $1/t^2$ at large t [26], consistent with perturbative quantum chromodynamics and anti-de Sitter/QCD counting rules, which in turn is consistent with what we do in the present context.

We also need the $C = -$amplitude, which can be calculated in terms of familiar single-photon form factors, and is taken as the corresponding muon pair amplitude times Dirac form factor $F_1(W^2)$.

Details of the calculation are given in the next section, which is divided into parts describing the kinematics, the massless pure QED limit, the continuation of the GPD analysis to the timelike region, and the actual calculation and results. A summary and conclusions are offered in Sec. III.

II. CROSS SECTIONS AND ASYMMETRY

A. Kinematics

The process is

$$e^+(p_{e^+}) + e^-(p_{e^-}) \to p(p_{h^+}) + \bar{p}(p_{h^-}) + \gamma(q'), \quad (2)$$

and for comparison, we also consider the same process with p and $\bar{p}$ replaced by μ^+ and μ^-, respectively.

The Mandelstam invariants can be defined as they are by Berends *et al.* [27], namely,

$$\begin{aligned} s &= (p_{e^+} + p_{e^-})^2, & t &= (p_{e^+} - p_h)^2, \\ u &= (p_{e^+} - p_{\bar{h}})^2, & s' &= (p_h + p_{\bar{h}})^2, \\ t' &= (p_{e^-} - p_{\bar{h}})^2, & u' &= (p_{e^-} - p_h)^2. \end{aligned} \quad (3)$$

Five of these variables are independent, and the sum is

$$s + t + u + s' + t' + u' = 4m^2, \quad (4)$$

where m is the mass of the hadron (or muon) in the final state, and we neglect the mass of the electron.

The cross section for process (2) is [14]

$$d\sigma = \frac{\beta W(s - W^2)}{64(2\pi)^5 s^2} |\mathcal{M}|^2 dW d\Omega^* d\Omega, \quad (5)$$

where $|\mathcal{M}|^2$ is the matrix element summed over final and averaged over initial polarizations and we also use the notations

$$s = q^2 = Q^2, \qquad s' = W^2, \qquad \beta = \sqrt{1 - \frac{4m^2}{W^2}}. \quad (6)$$

The solid angle Ω^* gives the direction of the outgoing proton or μ^+ in the $p\bar{p}$ or $\mu^+\mu^-$ rest frame and Ω gives the direction of the incoming electron in the e^+e^- rest frame. We define the z axis as the negative of the direction of the visible outgoing photon, and define the x axis from the transverse direction of the proton (or μ^+); see [14]. The angle between the proton or μ^+ and the outgoing photon will be θ^*, and the electron e^- will enter at angles (θ, ϕ) in the e^+e^- rest frame. Thus

$$d\Omega^* = 2\pi d(\cos\theta^*) d\Omega = d(\cos\theta) d\phi. \quad (7)$$

The momenta are conveniently given using two lightlike vectors p and n with the property $p \cdot n = 1$. Using these vectors,

$$\begin{aligned} q &= p_{e^+} + p_{e^-} = \frac{Q}{\sqrt{2}} p + \frac{Q}{\sqrt{2}} n, \\ \Delta &= p_h + p_{\bar{h}} = \frac{Q}{\sqrt{2}} p + \frac{W^2}{Q\sqrt{2}} n, \\ q' &= q - \Delta = \frac{Q^2 - W^2}{Q\sqrt{2}} n. \end{aligned} \quad (8)$$

In the e^+e^- rest frame,

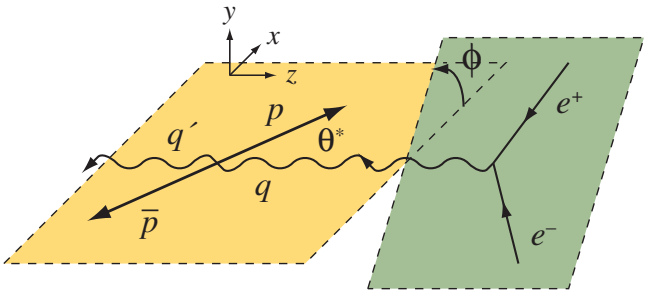

FIG. 3 (color online). Kinematics for radiative annihilation. This diagram is drawn for the $p\bar{p}$ rest frame. The angle θ is between the electron momentum and the z axis, but in the e^+e^- rest frame.

$$p = \frac{1}{\sqrt{2}}(1, 0, 0, 1), \qquad n = \frac{1}{\sqrt{2}}(1, 0, 0, -1), \quad (9)$$

while for the $p\bar{p}$ (or $\mu^+\mu^-$) CM one chooses

$$p = \frac{W}{Q\sqrt{2}}(1, 0, 0, 1), \qquad n = \frac{Q}{W\sqrt{2}}(1, 0, 0, -1). \quad (10)$$

In the $p\bar{p}$ (or $\mu^+\mu^-$) rest frame the proton or μ^+ momentum is

$$p_h = \tfrac{W}{2}(1, \beta\sin\theta^*, 0, \beta\cos\theta^*) \quad (11)$$

while the electron momentum in the e^+e^- CM is

$$p_{e^-} = \tfrac{Q}{2}(1, \sin\theta\cos\phi, \sin\theta\sin\phi, \cos\theta) \quad (12)$$

The kinematics is illustrated for the $p\bar{p}$ CM frame in Fig. 3.

The Mandelstam invariants t, u, t', and u' are given in terms of Q, W, and the angles by

$$\begin{aligned} t &= m^2 - \frac{W^2}{4}(1 - \cos\theta)(1 - \beta\cos\theta^*) \\ &\quad - \frac{Q^2}{4}(1 + \cos\theta)(1 + \beta\cos\theta^*) \\ &\quad - \frac{\beta Q W}{2}\sin\theta^*\sin\theta\cos\phi, \\ u &= (\text{same as } t \text{ but } \theta^* \to \pi + \theta^*), \\ t' &= (\text{same as } t \text{ but } \theta^* \to \pi + \theta^*, \theta \to \pi + \theta), \\ u' &= (\text{same as } t \text{ but } \theta \to \pi + \theta). \end{aligned} \quad (13)$$

B. The muon case at zero mass

Our calculations keep the nonzero mass of the final hadrons and are hence valid even when s is close to threshold. The analytic forms for the cross section and asymmetry for nonzero mass are rather long and we do not show them. However, the massless limit for the pure QED calculation, Fig. 4 is relatively simple and valuable as a benchmark.

The matrix element for $m = 0$, summed over final and averaged over initial polarizations, splits into a factor

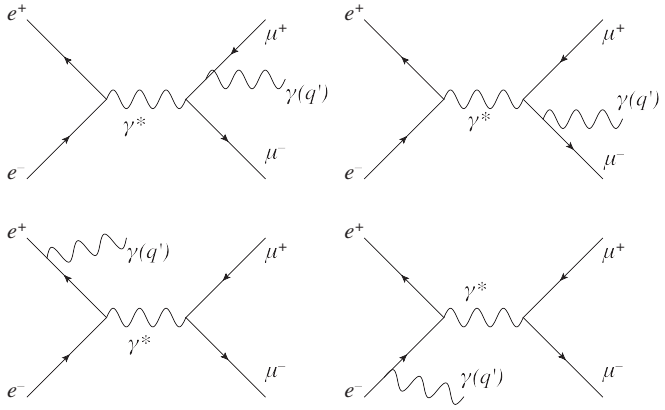

FIG. 4. Timelike DVCS in QED: radiative muon pair production.

related to the $2 \to 2$ process multiplied by a factor for the photon bremsstrahlung [27],

$$|\mathcal{M}|^2 = e^4 \frac{t^2 + t'^2 + u^2 + u'^2}{ss'} S, \tag{14}$$

with

$$S = e^2\left(\frac{s}{p_{e^+}\cdot q' p_{e^-}\cdot q'} + \frac{s'}{p_h\cdot q' p_{\bar{h}}\cdot q'} - \frac{t}{p_{e^+}\cdot q' p_h\cdot q'} - \frac{t'}{p_{e^-}\cdot q' p_{\bar{h}}\cdot q'} + \frac{u}{p_{e^+}\cdot q' p_{\bar{h}}\cdot q'} + \frac{u'}{p_{e^-}\cdot q' p_h\cdot q'}\right). \tag{15}$$

The simplicity of the above formula is a notable kinematic achievement, and more complicated earlier writings of the same quantity, for example, in [13], can be shown after the fact to agree with it.

We will give a sample result for the massless limit to show that the asymmetry we wish to observe can be quite large. The specific choices are: $\sqrt{s} = 8$ GeV, photon lab energy $|\vec{q}'|_{\rm lab} = 1$ GeV (using "lab" to mean the e^+e^- rest frame), all particles in the x-y plane, and a 90° angle between the entering electron and exiting photon in the lab. The photon lab energy is related to s and W^2 by

$$2\sqrt{s}|\vec{q}'|_{\rm lab} = s - W^2. \tag{16}$$

We plot in Fig. 5 the asymmetry

$$A_\mu = \frac{d\sigma(\mu^+) - d\sigma(\mu^-)}{d\sigma(\mu^+) + d\sigma(\mu^-)} \tag{17}$$

versus the angle $\theta_{e\mu}$ between the electron and positive muon in the lab (i.e., the lab analog of θ^*). This figure mimics one in [13] ($|\vec{q}'|_{\rm lab}$ here is $|\vec{k}|_{\rm lab}|$ there), and we have obtained it here both from Eqs. (14) and (15) above and from the massless limit of our full code. It shows that the asymmetry is close to 100% for a wide range of angles.

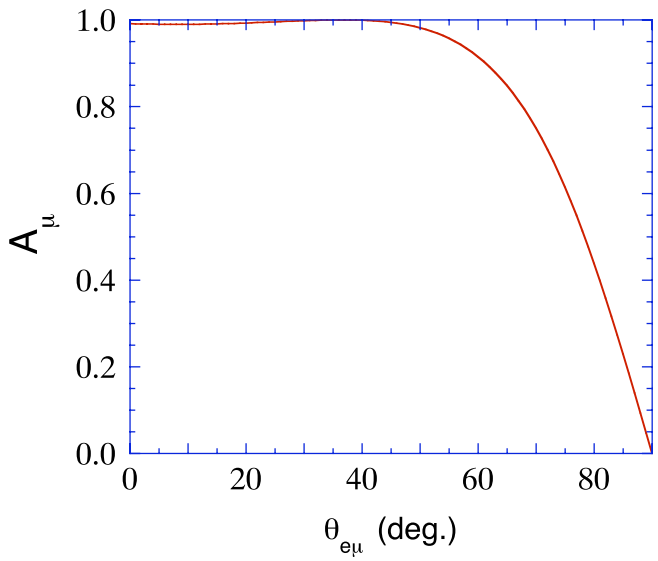

FIG. 5 (color online). Asymmetry where $\theta_{e\mu}$ is the angle between entering electron and exiting μ^+ in the electron-positron rest frame. Other variables are fixed as $\sqrt{s} = 8$ GeV, $|\vec{q}'|_{\rm lab} = 1$ GeV, $\theta = 90°$, and $\phi = 0$.

C. Timelike generalized parton distributions

In the Bjorken limit, $Q^2 \gg W^2$ and $q\cdot(p_h \pm p_{\bar{h}}) \gg W^2$, the analysis that relates deeply virtual Compton scattering to the generalized parton distributions [1,28] can be applied in the timelike case. The relevant diagrams at the partonic level for the C even case are shown in Fig. 6.

The antihadron in the final state can be thought of as a crossing of the initial state hadron from the usual DVCS.

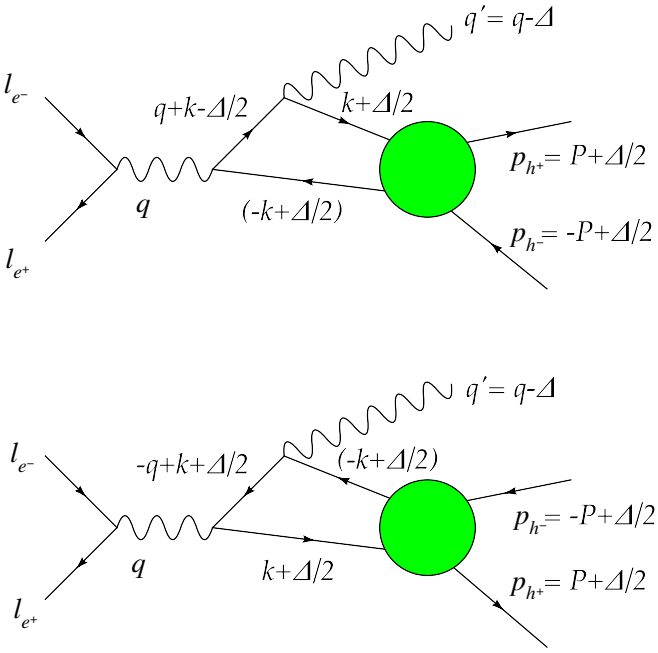

FIG. 6 (color online). Partonic diagrams for the case that the external photon is emitted from the hadrons.

Changing the appropriate sign from standard DVCS definitions, one has the momentum combinations

$$P = \tfrac{1}{2}(p_h - p_{\bar{h}}), \qquad \Delta = p_h + p_{\bar{h}}, \tag{18}$$

where $\Delta^2 = W^2$ and $P^2 = \bar{M}^2 = m^2 - W^2/4 \leq 0$.

The amplitude corresponding to Fig. 6 is

$$\begin{aligned}\mathcal{M}^{\mu\nu} = -e_q^2 \int d^4z \frac{d^4k}{(2\pi)^4} e^{ikz} \\ \times \Bigg[\gamma^\mu \frac{1}{\not{k} + \not{q} - \alpha \not{\Delta} + i\eta} \gamma^\nu \\ + \gamma^\nu \frac{1}{\not{k} - \not{q} + (1-\alpha)\not{\Delta} + i\eta} \gamma^\mu \Bigg]_{ab} \\ \times \langle p_h, p_{\bar{h}} | T \bar{\psi}_a(-\alpha z) \psi_b((1-\alpha)z) | 0 \rangle; \end{aligned} \tag{19}$$

α represents the freedom in choosing the loop momentum. For discussing timelike generalized distribution amplitudes, or generalized distribution amplitudes [16,29], we work in the Bjorken limit, and we choose a frame analogous to a standard choice for spacelike DVCS where the three-vectors for P and q are along the z axis but in opposite directions. We can do this with a suitable choice of the lightlike vectors p and n, and the momenta are expressed as

$$\begin{aligned} P &= p + \frac{1}{2}\bar{M}^2 n, \\ q &= 2\xi p + \frac{Q^2}{4\xi} n, \\ \Delta &= 2\xi' \left(p - \frac{1}{2}\bar{M}^2 n \right) + \Delta_\perp, \\ k &= xp + (p \cdot k) n + k_\perp, \end{aligned} \tag{20}$$

with $\xi' = \xi$ in the Bjorken limit. In the timelike case, ξ is limited in general by

$$\frac{1}{\beta} \leq \xi \leq \frac{Q}{\beta W}, \tag{21}$$

i.e., $\xi \geq 1$ in contrast to the spacelike case. Neglecting components that do not give large contributions in the Bjorken limit, the amplitude becomes

$$\begin{aligned}\mathcal{M}^{\mu\nu} &= \frac{e_q^2}{2}(g^{\mu\nu} - p^\mu n^\nu - n^\mu p^\nu) \int dx \left\{ \frac{1}{x + \xi + i\eta} + \frac{1}{x - \xi - i\eta} \right\} \bar{u}(p_h) \left[\not{n} H^q + \frac{i}{2m} \sigma^{\alpha\beta} n_\alpha \Delta_\beta E^q \right] v(p_{\bar{h}}) \\ &\quad - \frac{ie_q^2}{2} \varepsilon^{\mu\nu\alpha\beta} p_\alpha n_\beta \int dx \left\{ \frac{1}{x + \xi + i\eta} - \frac{1}{x - \xi - i\eta} \right\} \bar{u}(p_h) \left[\not{n} \gamma^5 \tilde{H}^q + \frac{n \cdot \Delta}{2m} \gamma^5 \tilde{E}^q \right] v(p_{\bar{h}}) \\ &\equiv -e_q^2 g_\perp^{\mu\nu} \bar{u}(p_h) \left(\not{n} R_V^q + \frac{i}{2m} \sigma^{\alpha\beta} n_\alpha \Delta_\beta R_T^q \right) v(p_{\bar{h}}) + ie_q^2 \varepsilon^{\mu\nu\alpha\beta} p_\alpha n_\beta \bar{u}(p_h) \left(\not{n} \gamma^5 R_A^q + \frac{n \cdot \Delta}{2m} \gamma^5 R_P^q \right) v(p_{\bar{h}}). \end{aligned} \tag{22}$$

We have used the definitions of the timelike analogs of the generalized parton distributions [30,31],

$$\begin{aligned} &\int \frac{dz^-}{2\pi} e^{ixp^+z^-} \langle p_h, p_{\bar{h}} | T \bar{\psi}_a \left(-\frac{z}{2} \right) \psi_b \left(\frac{z}{2} \right) | 0 \rangle_{z^+ = z_\perp = 0} \\ &= \frac{1}{4} \not{p}_{ba} \bar{u}(p_h) \left[\not{n} H^q + \frac{i}{2m} \sigma^{\alpha\beta} n_\alpha \Delta_\beta E^q \right] v(p_{\bar{h}}) \\ &\quad + \frac{1}{4} (\gamma_5 \not{p})_{ba} \bar{u}(p_h) \left[\not{n} \gamma^5 \tilde{H}^q + \frac{n \cdot \Delta}{2m} \gamma^5 \tilde{E}^q \right] v(p_{\bar{h}}). \end{aligned} \tag{23}$$

The arguments of H^q, E^q, $\tilde{H}^q$, and $\tilde{E}^q$ are (x, ξ, W^2). These arguments are standard when discussing GPDs, and the external variable ξ may of course be related to W and the angle θ^*. In the Bjorken limit,

$$\xi \approx \frac{Q^2}{4P \cdot q} \approx \frac{1}{\beta \cos\theta^*}, \tag{24}$$

for $\cos\theta^*$ not too small.

For somewhat different kinematics and for the pion case, one can also find timelike analogs of GPDs defined in [16,29].

The form factors R_V^q, R_T^q, R_A^q, and R_P^q are [32,33]

$$\begin{aligned} R_V^q(\xi, W^2) &= \int dx \frac{x}{x^2 - \xi^2 - i\eta} H^q(x, \xi, W^2), \\ R_T^q(\xi, W^2) &= \int dx \frac{x}{x^2 - \xi^2 - i\eta} E^q(x, \xi, W^2), \\ R_A^q(\xi, W^2) &= \int dx \frac{\xi}{x^2 - \xi^2 - i\eta} \tilde{H}^q(x, \xi, W^2), \\ R_P^q(\xi, W^2) &= \int dx \frac{\xi}{x^2 - \xi^2 - i\eta} \tilde{E}^q(x, \xi, W^2). \end{aligned} \tag{25}$$

The full amplitude will depend on

$$R_V(\xi, t) = \sum e_q^2 R_V^q(\xi, t), \tag{26}$$

with similar equations for $V \rightarrow T, A, P$.

As in the spacelike case, one can also relate the GPDs to the electromagnetic form factors, with the Dirac form factor given by

$$F_1(t) = \sum e_q \int dx H^q(x, \xi, t). \tag{27}$$

D. Hadronic model

The asymmetries, Eq. (1), arise from interference between the C-odd and C-even amplitudes. The hadronic vertex in the C-odd amplitude is the usual $\gamma p \bar{p}$ single photon vertex with Dirac and Pauli form factors evaluated at W^2, the four-momentum squared of the virtual photon for those diagrams.

In modeling the hadronic part of the C-even diagrams, we keep just the term $R_V(\xi, W^2)$. Further, recall that photon-hadron amplitudes can expect a $J = 0$ fixed pole, which would be a term with flat energy dependence and a form factor like dependence on the momentum transfer to the hadrons, W^2. We give R_V the same W^2 dependence as an electromagnetic form factor and normalize by

$$|R_V(\xi, W^2)| = \tfrac{4}{3} F_1(W^2). \tag{28}$$

The multiplicative factor is estimated from the expressions for $R_V(\xi = 0, W^2)$ and $F_1(W^2)$, Eqs. (25)–(27), and expecting domination by u-quarks and approximate mean momentum fraction $x \approx 1/2$.

Support for this normalization and shape comes from data on spacelike wide angle Compton scattering. The numerically most important form factor here is $R_V(t)$, and data shows that while $R_V(t)$ does drop less rapidly with increasing $|t|$ than $F_1(t)$, it does not do so by a lot, and that $R_V(t) = (4/3)F_1(t)$ is a decent representation of the data.

Further in our modeling, we note that the Lorentz structure that multiplies $R_V(\xi, W^2)$ in the Bjorken limit is the same as one obtains from the QED amplitude in the Bjorken limit. If we are not deeply in the Bjorken region, we can argue that the Lorentz structure of the amplitude is better represented by the QED amplitude, including the final fermion mass and multiplied by $R_V(\xi, W^2)$.

We use the above model and the R_V approximation of Eq. (28) in the calculations that give the plots shown in Fig. 7. Traces are done using FeynCalc and Mathematica, and integrations over a range of final state variables are done using Fortran and Vegas. (Note that our modeling of the timelike GPDs is rather different from [16].)

The asymmetries can be large when the kinematics are well chosen. Figure 7 shows two asymmetry plots, one at $s = 112$ GeV^2 relevant for Belle or *BABAR* energies and at $s = 14.3$ GeV^2 relevant for BEPC II energies. The asymmetries are for cross sections integrated over a stated range of angles, and plotted versus final hadronic mass W. Since

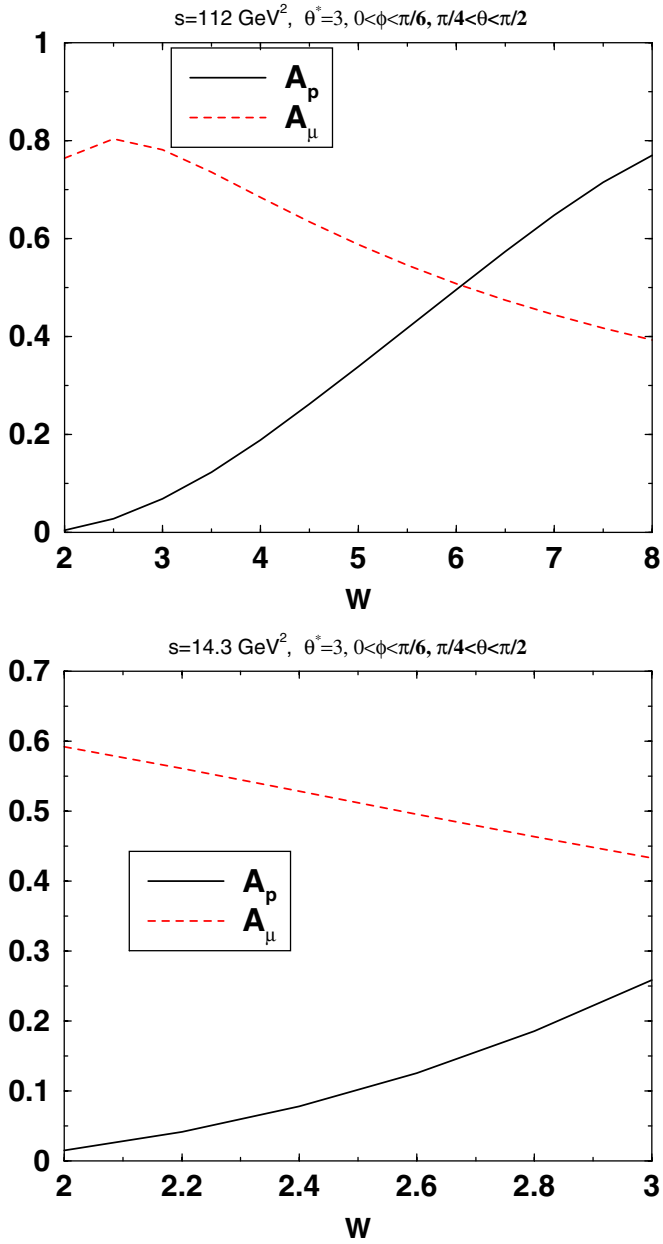

FIG. 7 (color online). Asymmetries for $\gamma^* \to \gamma p \bar{p}$ and its muonic counterpart, plotted versus the final fermion pair invariant mass, over a range beginning close to the $p\bar{p}$ threshold. The upper graph ($s = 112$ GeV^2) is for Belle or *BABAR* energies, and the lower graph ($s = 14.3$ GeV^2) is for BEPC II kinematics. The angles (in radians) and angular ranges are indicated on each plot.

the sign of the symmetry changes with ϕ, one should not integrate over more than half the range of that angle; if desired, one can integrate over fairly broad ranges of θ and θ^*. For comparison, and to indicate the mass sensitivity for the selected s and W, the plots also include the asymmetries expected for the purely muonic case.

To compare to a different model, we show in Fig. 8, the result from treating the C-even diagrams using only proton

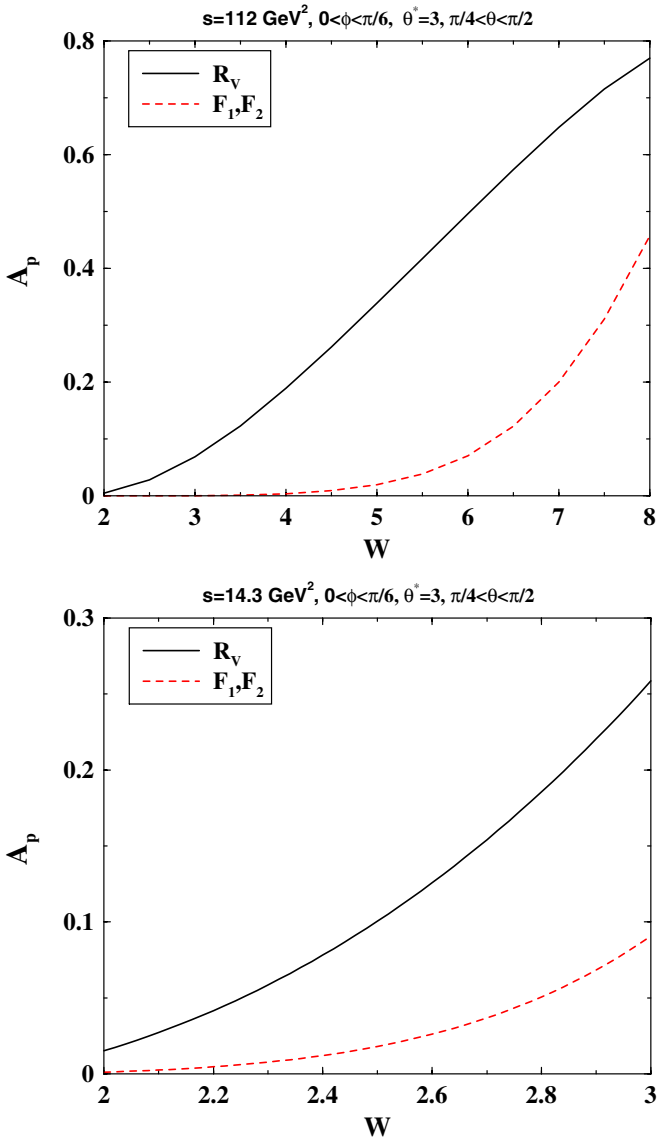

FIG. 8 (color online). Asymmetries for $\gamma^* \to \gamma p\bar{p}$ with the solid curve as in Fig. 7, using the C-even form factor $R_V(W^2)$ as described in the text, and the dashed curves calculated using a purely protonic model with form factors F_1 and F_2.

intermediate states, using Dirac and Pauli form factor structures at the two γpp vertices, and ignoring the extra form factors and extra form factor arguments that may appear when the intermediate proton is off shell. We keep the F_1^2 and F_1F_2 terms, where here in the dashed curves F_1 and F_2 are functions of q^2 and q is the four-momentum of the virtual photon, and show the results in two plots that are similar to Fig. 7 in that the energies are relevant to Belle (or *BABAR*) and BEBC II and the cross sections are integrated over a range of angles.

The charge asymmetries are largest when the outgoing photon is at a large angle to the line given by electron and positron momenta in the CM. Conversely, experiments that use radiative return to measure timelike form factors [20] often, though not invariably, keep the angle θ below 15° or above 165° in order to minimize contributions of final state radiation. The cross section drops about an order of magnitude as one changes θ from 15° to the 90° range, but the asymmetry increases, and the figure of merit (the cross section times asymmetry squared) stays roughly the same.

III. SUMMARY AND CONCLUSIONS

We have studied deeply virtual Compton production, $\gamma^* \to \gamma p\bar{p}$ in the timelike region. The production amplitudes can be $C = +$, where both photons couple to the hadrons, or $C = -$, where only one photon couples to the hadrons. Interference between them allows measuring one relative to the other, and can be isolated by considering forward-backward e^+e^- or $p\bar{p}$ asymmetry. We have used a simple model, wherein one Compton form factor, R_V, is kept and related to the Dirac form factor F_1 in a manner in agreement with data in the spacelike region. We have found that the asymmetry is quite large and measureable.

ACKNOWLEDGMENTS

We thank Markus Diehl, Dae-Sung Hwang, Felipe J. Llanes-Estrada, Bernard Pire, Adam P. Szczepaniak, and Werner Vogelsang for helpful discussions. A.A. thanks the U.S. Department of Energy for support under U.S. DOE Contract No. DE-AC05-06OR23177. S.J.B. thanks the U.S. Department of Energy for support under Grant No. DE-AC02-76SF00515. C.E.C. thanks the NSF for support under Grant No. PHY-0555600. A.M. thanks JLab, where part of the work was done, and also William and Mary, for hospitality and support.

[1] A. V. Radyushkin, Phys. Rev. D **56**, 5524 (1997); X. Ji and J. Osborne, Phys. Rev. D **58**, 094018 (1998); J. C. Collins and A. Freund, Phys. Rev. D **59**, 074009 (1999).
[2] S. J. Brodsky, M. Diehl, and D. S. Hwang, Nucl. Phys. **B596**, 99 (2001).
[3] M. Diehl, T. Feldmann, R. Jacob, and P. Kroll, Nucl. Phys. **B596**, 33 (2001); **B605**, 647(E) (2001).
[4] S. J. Brodsky, D. Chakrabarti, A. Harindranath, A. Mukherjee, and J. P. Vary, Phys. Rev. D **75**, 014003 (2007).
[5] S. J. Brodsky, D. Chakrabarti, A. Harindranath, A. Mukherjee, and J. P. Vary, Phys. Lett. B **641**, 440 (2006).
[6] M. Burkardt, Int. J. Mod. Phys. A **18**, 173 (2003).
[7] M. Burkardt, Phys. Rev. D **62**, 071503 (2000); **66**, 119903

(2002); J. P. Ralston and B. Pire, Phys. Rev. D **66**, 111501(E) (2002).
[8] D. E. Soper, Phys. Rev. D **15**, 1141 (1977).
[9] G. A. Miller, Phys. Rev. Lett. **99**, 112001 (2007); G. A. Miller, E. Piasetzky, and G. Ron, Phys. Rev. Lett. **101**, 082002 (2008).
[10] C. E. Carlson and M. Vanderhaeghen, Phys. Rev. Lett. **100**, 032004 (2008); Eur. Phys. J. A **41**, 1 (2009); Z. Abidin and C. E. Carlson, Phys. Rev. D **78**, 071502 (2008).
[11] S. J. Brodsky, F. E. Close, and J. F. Gunion, Phys. Rev. D **5**, 1384 (1972); **6**, 177 (1972); **8**, 3678 (1973).
[12] P. Kroll, M. Schurmann, and P. A. Guichon, Nucl. Phys. **A598**, 435 (1996); M. Diehl, T. Gousset, B. Pire, and J. P. Ralston, Phys. Lett. B **411**, 193 (1997); A. V. Belitsky, D. Muller, and L. Niedermeier, A. Schafer, Phys. Lett. B **474**, 163 (2000).
[13] S. J. Brodsky, C. E. Carlson, and R. Suaya, Phys. Rev. D **14**, 2264 (1976).
[14] Z. Lu and I. Schmidt, Phys. Rev. D **73**, 094021 (2006); **75**, 099902(E) (2007).
[15] J. P. Lansberg, B. Pire, and L. Szymanowski, Phys. Rev. D **73**, 074014 (2006).
[16] M. Diehl, T. Gousset, and B. Pire, Phys. Rev. D **62**, 073014 (2000).
[17] E. R. Berger, M. Diehl, and B. Pire, Eur. Phys. J. C **23**, 675 (2002).
[18] C. Amsler *et al.* (Particle Data Group), Phys. Lett. B **667**, 1 (2008).
[19] M. E. Biagini (SuperB Team Collaboration), J. Phys. Conf. Ser. **110**, 112001 (2008).
[20] W. Kluge, Nucl. Phys. B, Proc. Suppl. **181–182**, 280 (2008).
[21] S. J. Brodsky, F. E. Close, and J. F. Gunion, Phys. Rev. D **5**, 1384 (1972).
[22] S. J. Brodsky, F. E. Close, and J. F. Gunion, Phys. Rev. D **6**, 177 (1972).
[23] M. Creutz, Phys. Rev. D **7**, 1539 (1973).
[24] S. J. Brodsky, F. J. Llanes-Estrada, and A. P. Szczepaniak, Phys. Rev. D **79**, 033012 (2009).
[25] S. J. Brodsky, H. C. Pauli, and S. S. Pinsky, Phys. Rep. **301**, 299 (1998).
[26] A. Danagoulian *et al.* (Hall A Collaboration), Phys. Rev. Lett. **98**, 152001 (2007); A. Nathan, "*Workshop on Exclusive Reactions at High Momentum Transfer (including results from JLab experiment E99-114)*," Jefferson Lab 2007 (unpublished).
[27] F. A. Berends, R. Kleiss, P. De Causmaecker, R. Gastmans, and T. T. Wu, Phys. Lett. **103B**, 124 (1981); R. Gastmans and T. T. Wu, *The Ubiquitous Photon: Helicity Method for QED and QCD*, International Series of Monographs on Physics Vol. 80 (Clarendon, Oxford, United Kingdom, 1990), p. 648.
[28] X. D. Ji, Phys. Rev. D **55**, 7114 (1997); Phys. Rev. Lett. **78**, 610 (1997).
[29] M. Diehl, T. Gousset, B. Pire, and O. Teryaev, Phys. Rev. Lett. **81**, 1782 (1998).
[30] K. Goeke, M. V. Polyakov, and M. Vanderhaeghen, Prog. Part. Nucl. Phys. **47**, 401 (2001).
[31] M. Diehl, Phys. Rep. **388**, 41 (2003).
[32] A. V. Radyushkin, Phys. Rev. D **58**, 114008 (1998).
[33] M. Diehl, T. Feldmann, R. Jakob, and P. Kroll, Eur. Phys. J. C **8**, 409 (1999).